

Typicality of the 2021 Western North America Summer Heatwave

Valerio Lucarini

*Department of Mathematics and Statistics & Centre for the Mathematics of Planet Earth, University of Reading, UK **

Vera Melinda Galfi and Jacopo Riboldi

Department of Earth Sciences, Uppsala University, Uppsala, Sweden

Gabriele Messori

Department of Earth Sciences and Centre of Natural Hazards and Disaster Science (CNDS), Uppsala University, Uppsala, Sweden & Department of Meteorology and Bolin Centre for Climate Research, Stockholm University, Stockholm, Sweden

(Dated: December 16, 2022)

Elucidating the statistical properties of extreme meteo-climatic events and capturing the physical processes responsible for their occurrence are key steps for improving our understanding of climate variability and climate change and for better evaluating the associated hazards. It has recently become apparent that large deviation theory is very useful for investigating persistent extreme events, and specifically, for flexibly estimating long return periods and for introducing a notion of dynamical typicality. Using a methodological framework based on large deviation theory and taking advantage of long simulations by a state-of-the-art Earth System Model, we investigate the 2021 North America Heatwave. Indeed, our analysis shows that the 2021 event can be seen as an unlikely but possible manifestation of climate variability, whilst its probability of occurrence is greatly amplified by the ongoing climate change. We also clarify the properties of spatial coherence of the 2021 heatwave and elucidate the role played by the Rocky Mountains in modulating hot, dry, and persistent extreme events in the Western Pacific region of North America.

INTRODUCTION

Investigating the statistical properties of extreme meteo-climatic events and the physical mechanisms behind their occurrence is an area of ever-growing interest in climate science [32]. Additionally, their study allows to access some key aspects of the climate system, since there is in general a fundamental connection between extreme events and the dynamics of the system generating them [20, 22, 24, 31, 41]. Long-lasting meteo-climatic extremes are hazards of particular relevance because anomalous and persistent conditions are conducive to extremely damaging impacts on ecosystems and society [16, 32, 35, 56, 72]. Moreover, atmospheric phenomena with a long characteristic time scale are usually also characterised by a large spatial extent [26, 27], potentially leading to systemic risk [36]. In general, the occurrence of extremes of surprisingly large magnitude might be indicative of an approaching critical transition [18, 21].

The 2021 Western North America Heatwave Between late June and mid-July 2021 a large latitudinal band of the the western sector of North America faced a very intense heatwave, in the context of the ongoing megadrought in the region [75, 76]. Several new temperature records were established: 49.6°C were measured in Lytton, which is the new absolute temperature record for 2-m temperature (T2M) for Canada. It is estimated that the heatwave has led to over 1000 directly attributable deaths and damages worth several billion USD, associated with wildfires, crop loss, infrastructural damages,

and flooding due to rapid snow melt [39, 55, 67]. The record-breaking temperatures were the result of preconditioning combined with an anomalous atmospheric circulation. Prior to the heatwave, the southern portion of the region was anomalously dry [53, 55] and it is known that long-term drought increases the probability of occurrence of heatwaves, as a result of the drying of the soil [50, 61, 74], possibly leading to the onset of a cycle of heat, drought, and fire [38, 63]. This was compounded by the presence of an intense atmospheric Ω -block, like the one associated with the 2010 Russian heatwave [15, 23, 37]. Atmospheric blocks [73] are often the culprits for individual heatwaves as a result of possibly concurring processes, such as anomalies in clear-sky incoming radiation, warm air advection, and subsidence [5, 33]. The Western North America Heatwave (WNAHW) blocking developed on June 25th in association with a large scale pattern over the mid-latitudes dominated by low zonal wavenumbers [2, 67]. The ridge reached an impressive maximum 500 hPa geopotential height (Z500) of almost 6000 m over western North America. Figure 1 shows the ERA5 [29] T2M and Z500 anomaly fields averaged over periods of 7 and 15 days encompassing the heatwave. The agreement between the large scale patterns in Figs. 1a)-b) clearly shows the persistent and spatially coherent nature of the event. Predicting the onset of blocking is extremely challenging for numerical models [43, 47, 54] and, indeed, very few if any of the weather forecasting systems were able to estimate accurately the intensity of the 2021 WNAHW at lead times of a few weeks [39].

Recently, a team from the World Weather Attribu-

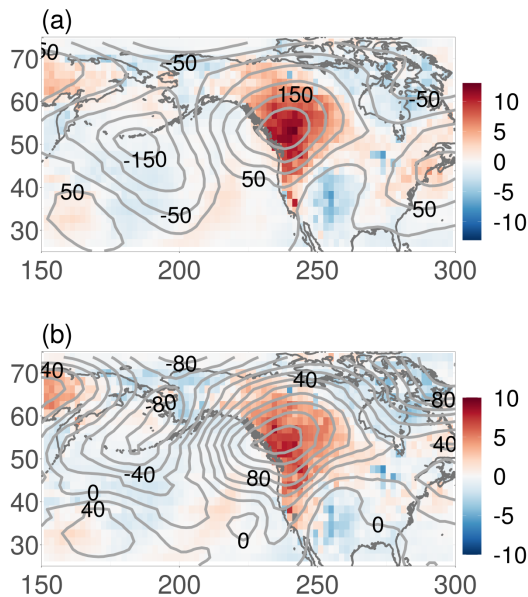


FIG. 1. ERA5 anomalies for (a) June 24th - June 30th 2021 and (b) June 24th - July 8th 2021 average of T2M (colours, in K) and Z500 (contour lines, in m) with respect to the 1991-2020 climatology for the corresponding period.

tion initiative has concluded, using a multi-model and multi-method attribution analysis applied to daily maximum temperatures, that it is possible to attribute almost non-ambiguously the 2021 event to climate change, because its likelihood in present climate conditions (factual world) is estimated to be orders of magnitude higher than in past climate conditions (counterfactual world) [55], according to the methodology presented in [28].

This Study In [23, 24] it was shown that large deviation theory (LDT) [69, 70] allows for constructing a climatology of heatwaves and cold spells over land. This approach is useful because one can go beyond purely descriptive statistics. Indeed, the return times of sufficiently persistent and intense temperature anomalies can be predicted by constructing the so-called rate functions for each given spatial location. For temperature time-series, such rate functions are to a good approximation quadratic. One can thus construct them, in close agreement with the central limit theorem, by using relatively simple statistics like the variability and integrated autocorrelation time of the daily temperature records.

It has recently become apparent that LDT can also be used to introduce a - somewhat counter-intuitive - notion of typicality of large and persistent temperature fluctuations associated with extreme heatwaves [23, 57, 58] or cold spells [23, 24]. The intense and persistent temperature fluctuations observed in a specific location are associated with a very unusual, rarely seen large-scale atmospheric configuration. Yet, if we subsample our dataset conditional on the occurrence of comparable tempera-

ture fluctuations in the same location, such large scale patterns are similar to each other, and are, in the sense discussed below, *typical*.

The main goal of this study is to investigate whether the 2021 WNAHW is dynamically typical according to the LDT viewpoint presented in [23, 24], *i.e.* whether the corresponding large-scale circulation pattern can be considered to belong to the subset of typical circulation patterns mentioned above. We will also try to better understand the geographical features of the 2021 WNAHW by elucidating its spatial coherence. This study also presents a more detailed and critical account of the methodology presented in [23], which supports its robustness.

Note that, through the use of an Earth System Model run in preindustrial, steady state configuration as in [23], we will study the event as a fluctuation with respect to a baseline climatology. Hence, our approach is different from that of the attribution studies mentioned before, where what matters is the absolute temperature reading, rather than the anomalies. We will estimate the impact of shifting the climatology in order to roughly account for the impact of historical climate change on the probability of occurrence of events comparable to the 2021 WNAHW. While this is obviously a serious simplification, because one neglects all the possible impacts of shifting climate conditions on climate variability (e.g. changes in the dynamics of the atmosphere, water cycle, soil properties [5]), shifting the climatic mean has been shown to be a good first order approximation of the impact of climate change on the statistics of heatwaves [67].

The 2021 WNAHW featured a particularly acute phase between June 27th and June 29th. Hence, some studies have focused on the statistical investigation of daily temperature records [55, 67] and taken advantage of the statistical framework provided by extreme value theory [9, 41]. Since persistence plays a major role in determining the impact of heatwaves [56], we prefer to look into cumulative temperature anomalies.

A succinct account of the relevant LDT background that supports our analysis is presented in the next section. This is then followed by the discussion of the main findings of this investigation. A section presenting the concluding remarks and the perspectives for future investigation concludes this contribution. This letter is accompanied by supplementary material (SM)[42] that complements the core findings described here.

THE MATHEMATICAL BACKGROUND

We follow below the viewpoint developed for fluid flows in [10, 11], which is based upon the theoretical framework presented in [8]. We consider a continuous-time chaotic dynamical system defined by an ordinary differ-

ential equation of the form

$$\dot{x} = G(x) \quad (1)$$

with $x \in \mathbb{R}^N$ with initial condition $x(0) = X$ belonging to the attractor Ω of the system. The solution at time $t \geq 0$ is given by $x(t, X) = S^t X$ where S^t is the evolution operator up to time t . We assume that the system possesses a unique physical invariant measure ρ supported on Ω and that our initial condition $X \in \Omega$, *i.e.* all transients have died out and we are in steady-state conditions. We now introduce a target function of the form $F(\tau, X) = \int_0^\tau dt f(x(t, X))$ where f is a smooth function of its argument. Such a target function can be tailored to capture the persistent extreme of interest. We define as $\mathcal{P}(F(\tau, X) > z)$ the probability that $F(\tau, X)$ has value larger than z . The working hypothesis is to be able to write $\mathcal{P}(F(\tau, X) > z)$ in the limit of large z as a large deviation law of the form

$$\mathcal{P}(F(\tau, X) > z) \asymp \exp\left(-\min_{X \in A_{F,\tau,z}} I(X)\right) \quad (2)$$

where $A_{F,\tau,z}$ is the set of points of Ω such that if $y \in A_{F,\tau,z}$, then $F(\tau, y) > z$ and \asymp indicates that the ratio of the logarithms of the two sides tends to 1. Finally, $I(X)$ is the so-called rate function. As a result, one obtains that

$$\mathcal{P}(F(\tau, X) > z) \asymp \exp(-I(X^*(z))),$$

where

$$X^*(z) = \arg \min_{X \in A_{F,\tau,z}} (I(X)).$$

This implies that the most likely way the event $\mathcal{P}(F(\tau, X) > z)$ occurs is for $X = X^*(z)$. Namely, as we consider larger and larger thresholds z , the probability measure concentrates more and more around a specific initial condition $X^*(z)$. Let's provide an interpretation of this result following [8]. The initial conditions $X = X^*(z)$ around which the measure concentrates define the forward trajectory $x(t, X^*(z)) = S^t X^*(z)$. It is clear that such initial condition and the ensuing forward trajectory are extremely atypical exactly because there is an association with the desired rare event defined in the limit of large z . Conversely, if one studies the statistics of the system conditional on the occurrence of the rare event (*i.e.* restricted to the set $A_{F,\tau,z}$), the trajectory departing from $X^*(z)$ becomes typical. Indeed, LDT captures here the least unlikely of all the unlikely ways the rare event of interest can occur [12].

In the previous studies of the 2010 Russian Heatwave, 2010 Mongolian Dzud (an extreme cold spell), and 2019 North American cold spell [23, 24] the model-simulated events selected according to the procedure above, where z was a measure of the observed extreme event at a given location in its core region

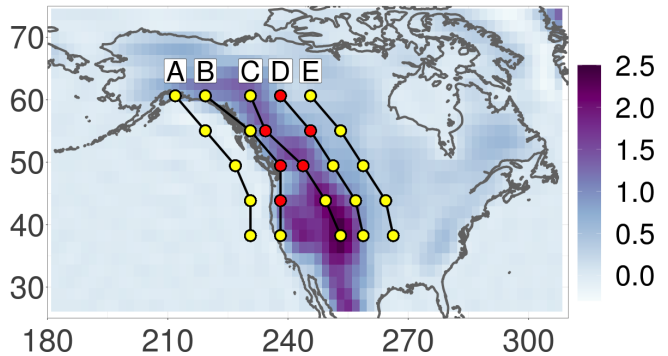


FIG. 2. The slanted grid shows the location of the 25 grid points considered in this study. They are arranged in an orography-following fashion and for latitudes ranging from $38^\circ N$ to $61^\circ N$. The red dots indicate the core of the 2021 WNAHW as discussed in the text. The color bar indicates the MPI-ESM-LR model orography in units of Km.

1. resembled each other: the large scale spatial patterns of T2M and Z500, while being abnormal in reference to the climatology, were highly correlated with the mean field computed by averaging over the various events;
2. resembled the actual historical event: the observed T2M and Z500 fields could be interpreted as being drawn from the same distribution including the various model-generated surrogate events.

The properties 1. and 2. above indicate the usefulness of the mathematical framework given in the previous section: if we consider events selected according to a sufficiently stringent constraint, they can be seen as fluctuations around the optimal $x(t, X^*(z)) = S^t X^*(z)$ case, which can be estimated as the average over all the selected events generated by the model [10, 11].

DATA

We use here, on top of the T2M and Z500 ERA5 [29] fields for June 24th - July 8th 2021, the data for the same variables gathered from a 1000-year simulation performed by the MPI-ESM-LR version 1.2 Earth System Model (ESM) [48] in standard pre-industrial conditions in terms of atmospheric composition and land-use dataset (*piControl* run). This ESM is among the best performing models participating to the 6th phase of the Climate Model Intercomparison Project (CMIP6) [17], just as its previous version was among the best performing CMIP5 models [4].

After removing the seasonal cycle by subtracting the climatology of each day of the year, we select for each year an extended summer lasting 160 days and beginning on May 5th, as in [23], in order to remove winter

heatwaves from the statistics. We consider 25 grid points located in the Western part of North America; see Fig. 2. These grid points are arranged in an irregular lattice: the North/South direction is distorted in such a way that it approximately follows the orography. The grid points are defined by their latitude (38° N- 61° N in steps of $\approx 6^\circ$) and by the letters A, B, C, D, and E (from west to east). A refers to points located over the ocean (except in case of latitude 61° N), not far from the coast; B to points located near the Pacific coast; C and D to points at the top and at the eastern flank of the Rocky mountains; and E to points located in the continental region to the East of the Rocky mountains.

Following the mathematical framework described above, the first step is to use the following definition for the target function: $F_k(\tau, X) = \int_0^\tau dt(T_k(t, X) - \bar{T}_k^\tau)$, where k is the index referring to the grid point of interest, $T_k(t, X)$ is the T2M at time t given the initial condition X , and \bar{T}_k^τ is the long-term climatology of T_k . During the 2021 event, for both cases of $\tau = 15 d$ and of $\tau = 7 d$, the target function is largest at the following grid points (indicated in red in Fig. 2): 44B (near Portland, USA), 49B (near Vancouver, Canada), 49C, 55D (Calgary, Canada, is approximately midway between these two latter locations), 55C, and 61D (near Forth Smith, Canada). See Tables I and II.

RESULTS

In what follows we show that there is a clear signature of the 2021 WNAHW in the natural variability of the MPI-ESM-LR. We will further test whether there is evidence of a strong signature of the Rocky Mountains on the 2021 WNAHW. Indeed, orography has a key role in catalyzing and determining the location of large scale and persistent weather patterns associated with the low-frequency variability of the atmosphere [3, 6, 7, 44, 51, 52, 59, 60] and in determining the properties of heatwaves [33, 34].

The 1000-year MPI-ESM-LR model run features by and large events comparable to the 2021 WNAHW in terms of observed anomalies. The return times for values of the target function at the locations indicated above range from multidecadal to multicentennial. In the case $\tau = 15 d$, they reach a value of 200 y at grid point 49C and at 91 y at grid point 55D. In the case $\tau = 7 d$, one gets multicentennial values at grid points 49B and 49C. Instead, the model cannot find an event of intensity equal or larger than the 2021 WNAHW for grid point 55D. Comparing Tables I and II one finds confirmation of the presence of a very intense phase within the heatwave, as already mentioned in the Introduction. For the other grid points shown in Fig. 2 and not included in Tables I and II, instead, the return times of the 2021 value of $F_k(\tau, X)$ estimated through the MPI-ESM-LR model dataset are

Grid point	RL_{50}	$\Delta T2M$	$RT(\Delta T2M)$	$RT(\Delta T2M - \delta)$
44B	6.3	5.6	19	6
49B	6.0	5.4	22	5
49C	5.6	6.2	200	22
55C	7.3	6.7	29	8
55D	5.2	5.5	91	17
61D	5.7	5.3	30	6

TABLE I. Surface temperature anomalies ($\Delta T2M$, in $^\circ C$) averaged over $\tau = 15 d$ for the 2021 WNAHW at selected grid points (see Fig. 2) in its core region (third column). For each grid point, we have $\Delta T2M = F_k(\tau, X)/\tau$. The corresponding return times (RTs, in y) estimated with the MPI-ESM model (fourth column) as well as the the RTs for the climatology shifted by $\delta = 1.2^\circ C$ (last column) are reported. The model return levels for 50-year return times (RL_{50} , in $^\circ C$) are reported in the second column.

grid point	RL_{50}	$\Delta T2M$	$RT(\Delta T2M)$	$RT(\Delta T2M - \delta)$
44B	8.8	8.2	29	8
49B	8.4	9.7	333	53
49C	7.6	8.9	500	62
55C	10	9	21	9
55D	7.2	9.1	> 1000	1000
61D	7.9	7.5	36	9

TABLE II. Same as Table I, but for $\tau = 7 d$.

at most of the order of few years. Hence, they are relatively (or very) common within, e.g., a 30-year time span commonly used to benchmark climatology. We conclude that the red grid points in Fig. 2 define the (vast) core region of the 2021 event, which results to be larger than the area investigated in [55, 67].

Robustness of the Methodology We first test whether the mathematical framework presented above provides us with a robust and practically usable methodology. We proceed as follows. As shown in Tables I and II, the 50-year return level estimated by the model is by and large a good reference value for the observed anomalies for all of the grid points of the core region of the 2021 WNAHW. The results are weakly dependent on the specific choice of the return time, as long as it is sufficiently long; see discussion below. We then select, for each of the 25 grid points shown in Fig. 2, as threshold z_k for $F_k(\tau, X)$ the 50-year return level. In such a way, we have a homogeneous statistics throughout the domain of interest for extreme heatwaves, because we identify $J = 20$ events for each of the 25 grid points of interest. Each event corresponds to one initial condition X^j compatible with $F_k(\tau, X) > z_k$. In other terms, our procedure aims at defining candidates for weather analogues [40, 71, 77] for the extreme event of interest. We present below results for $\tau = 15 d$. All the main conclusions we draw are valid also for $\tau = 7 d$, whose corresponding figures are shown in the SM; see further discussion therein.

We first test whether by considering for a given k such a high threshold z_k for the function $F_k(\tau, X)$ we end up

identifying sufficiently similar weather patterns, which can be seen as fluctuations around $X^*(z)$. This amounts to being able to introduce a notion of typicality for such extreme events that leads to identifying good weather analogues.

The cyan boxplots in Fig. 3 show the properties of the spatial correlation between the τ averages of T2M and Z500 fields of the $J = 20$ events selected for each grid point k and their respective mean. Since we are now testing the robustness of the methodology, we perform this analysis for all the grid points shown in Fig. 2.

The spatial correlation is computed over the region $[20^\circ \text{ N}, 75^\circ \text{ N}] \times [150^\circ \text{ E}, 300^\circ \text{ E}]$, which includes the whole North America, approximately half of the North Pacific ocean, and a quarter of the North Atlantic ocean. The results shown below are very weakly sensitive to adjustments in the boundaries of such a (vast) region. We clearly see that in most cases the mean of spatial correlation is high, with a moderate standard deviation, which indicates high coherence between the events. In general, the coherence is higher as we focus on higher latitudes, thus reducing the impact of tropical dynamics, and as we move away from the ocean towards the Rockies, in agreement with what is mentioned above regarding the interaction between orography and low-frequency (and large scale) mid-latitude atmospheric variability.

Stronger support to these statements can be found by looking at the Taylor [65] diagrams shown in the SM as Figs. S3-S4 (S5-S6) for the T2M (Z500) field, 15-day and 7-day averages, respectively. Taylor diagrams allow for a more complete comparison between fields by including, on top of their spatial correlations, also the centered root-mean-square (RMS) difference and the amplitude of their variations (represented by their standard deviations). For most of the 25 grid points of interest, the 20 50-y return level events define a cluster - see below - characterised by high correlation and low centered RMS difference with respect to the mean of such events.

We remark that for the grid points over the ocean (where the correlation of T2M has a slower decay) and in case of the southernmost latitude (where there is strong interaction between tropical and extratropical dynamics), the spread is substantially larger because it is more difficult to obtain a well-defined typicality there [23].

Clearly, because of averaging, the mean tends to have lower standard deviation than the individual events. As we consider longer and longer return times - see Figs. S7-S10 in the SM - the clusters become better defined as the individual events become more and more similar to their averages. Indeed, in each Taylor diagram the center of the cluster moves in the direction of the reference point in the x-axis. The presence of a single well-defined statistical cluster for the T2M and Z500 fields (separately and taken together) is confirmed in all cases for fields constructed for grid points over land and for return times longer than 20 years through the gap statistics [68] for

Gaussian mixture models [49], which has been evaluated using the MATLAB function `evalclusters` [46].

We conclude that the methodology followed here allows us to distill the fundamental properties of heatwaves throughout the domain of interest. The test above is not complete because, for each k , one should look at the agreement between the evolution up to time τ of the various $j = 1, \dots, J$ initial conditions X^j . Instead, here we are looking at the agreement between the fields $\bar{X}_\tau^j = 1/\tau \int_0^\tau dt S^t X^j$, and we estimate $\bar{X}^*(z)_\tau = 1/J \sum_{j=1}^J \bar{X}_\tau^j$. Nonetheless, the results we obtain are extremely encouraging.

Fingerprinting the 2021 WNAHW The next step is to discover whether there is an agreement between the heatwaves constructed as above and the 2021 WNAHW. Indeed, if we repeat the analysis by using the actual return levels of the 2021 WNAHW - see gray boxplots in Fig. 3 - we obtain for the grid points in the core region results that are in very good agreement with what found using the 50-y return levels. This confirms that the estimate of $X^*(z)$ depends weakly on z_k as long as we are choosing a sufficiently large value for z_k .

The full dots in the gray boxplots in Fig. 3 show, for each k , the value of the spatial correlation coefficient between the estimate of $\bar{X}^*(z)_\tau$ and the actual τ -averaged ERA5 fields depicted in Fig. 1. The spatial correlation coefficient for both the T2M and Z500 field is highest when considering the events constructed for the grid points defined in Tables I and II. For five out of these six grid points, additionally, we have that the value of the spatial correlation coefficient is within the range of values obtained between \bar{X}_τ^j and $\bar{X}^*(z)_\tau$, and in most cases within the one standard deviation interval. Hence, the ERA5 anomaly field can be seen as belonging to the same statistical ensemble as the anomalies produced by the model, given the stringent criteria set for suitably choosing the corresponding events. The only exception comes from the grid point 49C, basically because we have only few model occurrences of heatwaves of larger intensity than the 2021 WNAHW. Such events closely resemble each other, so that the range of values of correlations with their average is very small. Nonetheless, the spatial correlation between the estimated $\bar{X}^*(z)_\tau$ and the actual τ -averaged ERA5 is high. The Taylor diagrams shown in Fig. S11 (T2M) and Fig. S13 (Z500) of the SM further support these conclusions. Similar results are obtained when considering $\tau = 7 d$ (see Figs. S12 and S14 of the SM), except for the fact that the ensemble is too limited to draw conclusions for the grid points 49B and 49C, and no ensemble members are available for the grid point 55D, possibly as a result of the model's inability to reproduce specific local processes.

The similarity of the six panels of Fig. 4 among themselves, with Fig. 1b, and with the corresponding panels of Fig. S16 of the SM (which are constructed using the ac-

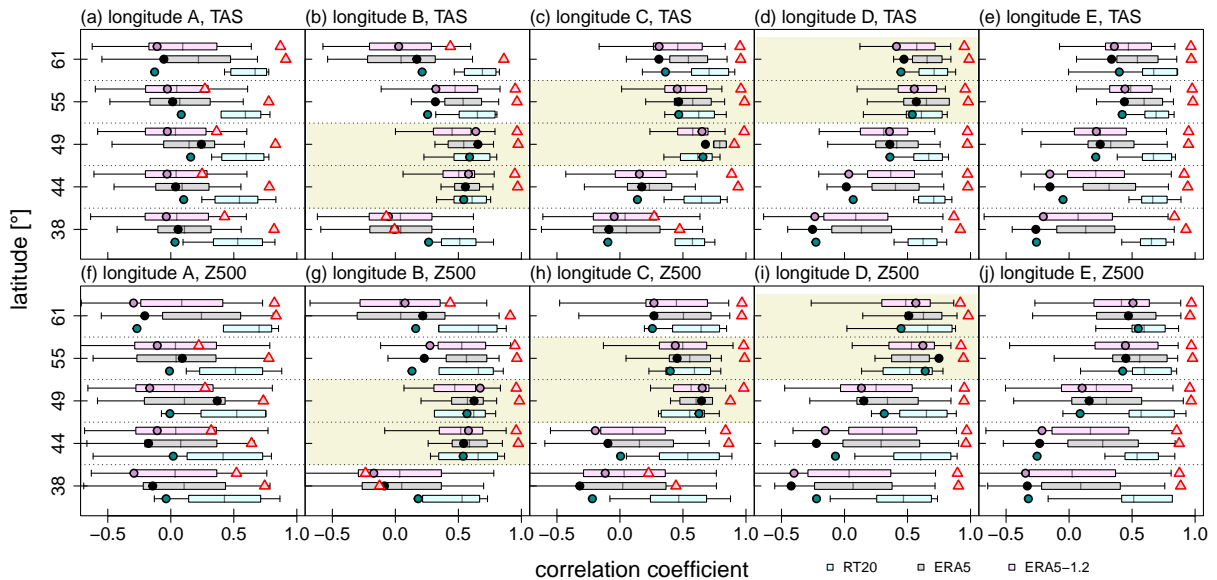


FIG. 3. Spatial correlation coefficients between the model-simulated events and their mean for the T2M (a-e) and Z500 (f-j) fields. The coefficients are obtained for events selected by defining a high threshold in the cumulated temperature anomaly at the corresponding grid point over $\tau = 15$ d; see indication of the latitude on the side and of the longitude on top. The shading indicates the core region of the 2021 WNAHW, see Tables I-II. In each subpanel, the boxes refer to the $\pm 1\sigma$ interval, and the whiskers indicate the full range of results. The dots indicate the spatial correlation coefficient between the mean of the model runs and the corresponding field from ERA5. Additionally, i) Cyan refers to 50-y return time events, ii) Gray refers to events with return level corresponding to the one of the 2021 WNAHW, and iii) Magenta refers to events where the return level of 2021 WNAHW event is reduced by $\delta = 1.2^\circ\text{C}$. The triangles indicate the spatial coefficient between the mean of the events i) and the mean of the events ii) and iii), respectively. See the Taylor diagrams in Figs. S3-S14 in the SM for more complete information on the agreement between the considered patterns.

tual return levels of the 2021 WNAHW) provides a visual confirmation of what mentioned above. In meteorological terms, the possibly most striking common features between the model data and the actual 2021 WNAHW are a) the presence of a wavetrain across the Pacific ocean [39], which closely resembles the anomaly pattern deemed responsible for drought over California [66]; and b) the powerful ridge in the mid-latitudes extending from the Pacific over the Rockies, which reminds of the pattern that which is associated with the occurrence of intense drought in the Western US [62, 64, 66, 76].

We are now able to strengthen the statement made before regarding the fact that the grid points included in Tables I and II correspond to the core of the 2021 WNAHW, which was based purely on the intensity of the local T2M anomalies. For these six grid points we have both high internal coherence among the model-generated events and high statistical compatibility with the large-scale fields of the 2021 WNAHW. Geographically, these grid points correspond to a region stretching approximately in the SSW-NNE direction and, hence, shifting from the coastal area to the eastern side of the Rockies as one progresses northwards. These grid points define a coherent region associated with a very special yet very robust feature of the natural variability of the cli-

mate, which most recently manifested itself as the 2021 WNAHW. As can be seen by comparing the corresponding panels of Figs. S2 and S16, for each of these grid points the average pattern of the model-generated events is virtually unchanged if we consider either a) the 20 events leading to the largest local persistent temperature anomaly (also portrayed in Fig. 4) or b) events leading to local persistent temperature anomalies equal or larger than what observed during the 2021 WNAHW. Such an agreement can also be checked by noting that for such grid points the triangles next to the grey boxes in Fig. 3 are located very close to one.

Let's look at the grid points outside the 2021 WNAHW core region. The gray boxplots, constructed according to the 2021 WNAHW return levels, cover a larger range of values and are substantially shifted towards lower values compared to the corresponding cyan ones. This means that if we select soft extremes (or events that are not extreme at all), the notion of typicality discussed above is lost, because we are outside the regime where LDT applies. The Taylor diagrams indicate a much reduced agreement between the average of the model generated T2M and Z500 fields and the corresponding ERA5 fields as compared to the case of the core region.

Specifically, from Fig. 3 and Figs. S3-S6 of the SM, one

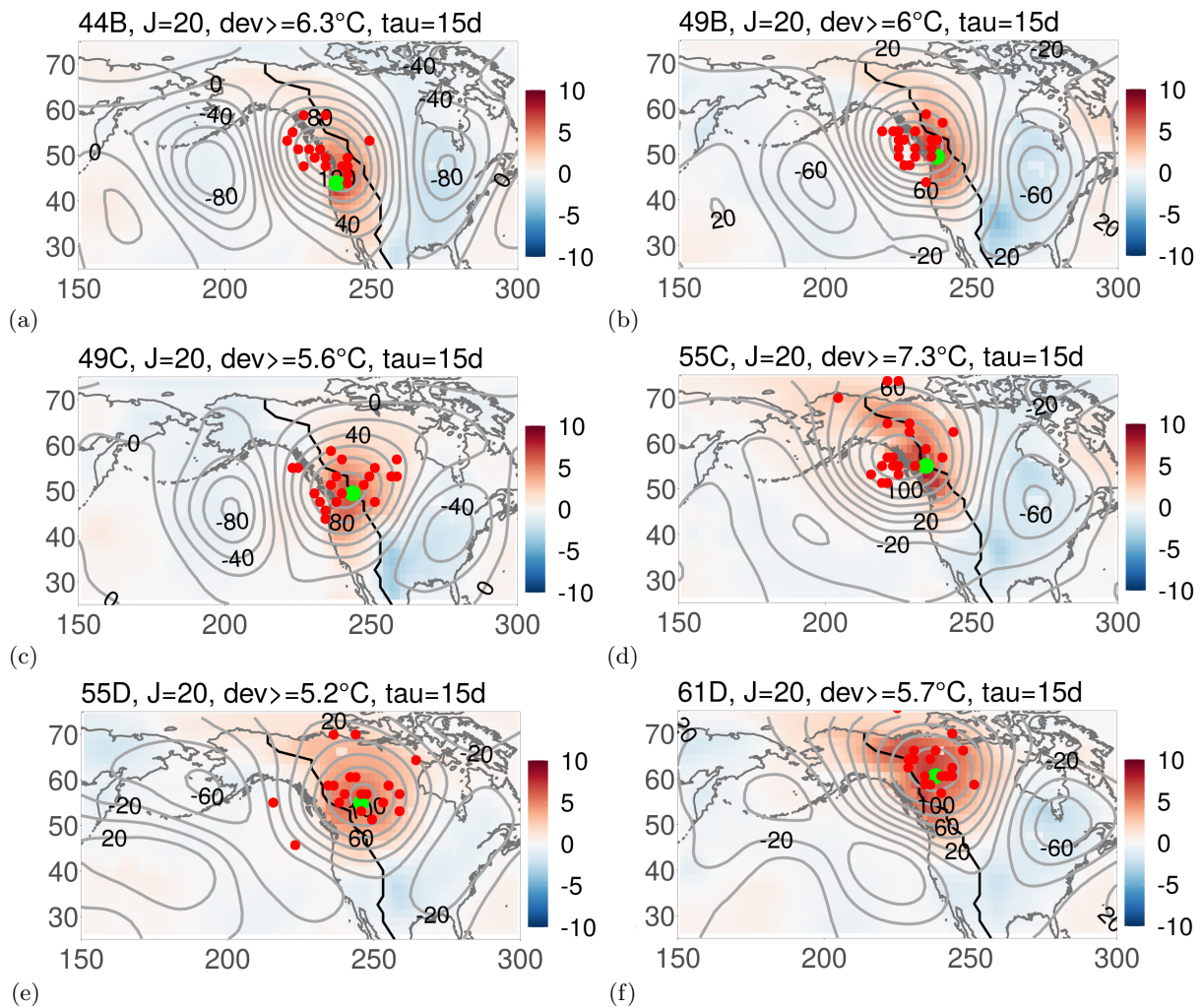


FIG. 4. T2M and Z500 anomaly fields (averaged over $\tau = 15$ d) computed as means over the $J = 20$ most extreme model-simulated events chosen according to a high T2M anomaly thresholds at grid points 44B (a), 49B (b), 49C (c), 55C (d), 55D (e) and 61D (f). The red dots indicate the center of the high pressure for each of the J events. All the patterns look remarkably similar, and similar to the 2021 WNAHW, see Fig. 1.

can see that a good agreement still exists while considering averages constructed for grid points to the NNE of the core region, such as 55E and 61E. Instead, the correlation dramatically decreases when considering grid points geographical close to the core region, such as 44C and 55B, but off-axis with respect to the SSW-NNE direction. Hence, at least in the MPI-ESM-LR model world, heatwaves centred in, e.g., grid points 44C and 55B are due to dynamical processes that are fundamentally different from those responsible for the 2021 WNAHW.

DISCUSSION AND CONCLUSIONS

The 2021 WNAHW shocked experts and general audiences around the world and had devastating impacts on a large swath of land in North America. We have investigated this event following the strategy delineated

in [23, 24] and based upon the theoretical framework defined in [8, 11]. While the 2021 WNAHW is very rare and unusual according to the overall statistics of weather variability, it becomes *typical* when considering the statistics conditional on the validity of a specific constraint, namely the occurrence of a large and persistent summer temperature anomaly at one specific location, defined by a grid point of our model. Typicality results, against intuition, exactly from *the extreme intensity* of the event. Indeed, we find a good agreement, as shown by Fig. 3 and by the Taylor diagrams included in the SM, between the large scale meteorological anomaly patterns of the 2021 WNAHW and those of the events selected from the 1000-year-long MPI-ESM-LR preindustrial run according to the procedure above when considering any grid point located in a specific region of Western North America. This region has an extension of 2000 Km in the SSW-NNE di-

rection and defines the core of the 2021 event.

This indicates that the circulation pattern causing heatwaves over this region in the model resembles the one that caused the 2021 WNAHW, at least in the spatial distribution of mid-tropospheric and surface anomalies. This also indicates that, at least in the model climate, there is, roughly speaking, mainly one way to get heatwaves of such large magnitude in that region.

The obtained large scale patterns are in good correspondence with those deemed responsible for the persistent drought in the western US. This supports the existence of a cascading process acting across different spatial and temporal scales that is increasing dramatically climate risk in the western sector of the North American continent, with conditions being and becoming particularly exacerbated in California [1, 14, 45].

Modulating the imposed threshold on the local T2M anomaly amounts to taking into account, in first approximation, changing background climatic conditions. Shifting the mean has been recently shown to represent a good first approximation for evaluating the statistics of hot temperature extremes in a changing climate [25, 67]. This can be explained - in the case of persistent extremes - by the fact that the rate function for summer (as opposed to winter) temperature near the region of interest seems to be approximately insensitive to the levels of CO_2 [23]. We find - see Tables I-II - that in the core of the 2021 WNAHW the return times of events comparable to the 2021 event decrease substantially (by a factor of about 3 to 10) if one budgets in an offset ($\delta = 1.2^\circ C$) that approximately represents the historical shift of temperatures due to the realized climate change between pre-industrial conditions and today. This indicates that the likelihood of events comparable to the 2021 WNAHW is greatly enhanced by climate change: a very or extremely unusual event becomes comparably likelier. Interestingly, in the core region the typicality of the extreme events is maintained even if we relax a bit our procedure: the large scale meteorological patterns associated with events selected according to the less stringent (because of the offset) constraint imposed in the core region are in good agreement with those obtained using the more stringent criterion; see the magenta and gray boxplots in Fig. 3.

The mathematical setting behind this paper indicates why dynamical similarity exists between the various extreme events, despite their different intensity, as long as they are all chosen according to the same sufficiently stringent constraint. Our analysis is limited in scope by the fact that we look at the data produced by only one state-of-the-art ESM - yet a model with rather good overall skill as compared to the others included in the CMIP6 exercise [17], and at least some of our conclusions could be affected by its biases and deficiencies. It would be important to test whether similar results can be found in other CMIP6 models, also taking into account that ESMs tend to globally underestimate duration, intensity, and

frequency of heatwaves, yet having a comparatively better performance in the West North America region [30]. Interestingly, the CMIP6 bias is instead on the warm side for daily temperature maxima [13], which further reinforces the need to deal carefully with the property of persistence when looking at hot events. The methodology adopted here could be replicated for studying the statistics and dynamics of several historical extreme heatwaves, taking advantage of the dataset compiled by [67].

In order to better characterize the features of the event studied here - with the goal, e.g., of better understanding the separate role of dynamical and thermodynamical contributions, preconditioning factors, and the role of teleconnections - one would need larger statistical sets than those considered here, because we construct our ensembles by imposing rather stringent conditions on the fields. A possible strategy is to take advantage of the CMIP6 dataset [17], and use all available ensemble members and various climate scenarios in order to address the problem of the impact of climate change on the statistics and dynamics of heatwaves. A theoretically more challenging yet more promising strategy is, instead, to exploit rare events algorithms to disproportionally populate the exotic configurations of interest and learn a great deal more about them [57, 58]. Nonetheless, both of these directions are beyond the scopes of this investigation as they require extensive data analysis and modelling work.

Our approach can also be seen as leading to the definition of weather analogues for extreme events. In [19] it was shown, by investigating the recurrence of weather analogues, that in the last decades there has been a positive trend in the frequency of occurrence of atmospheric circulation patterns over the North Atlantic driving summertime dryness and heatwaves and a negative trend in those leading to wet, cooler summer conditions across Europe. We envision applying the methodology proposed in [19] to the West North America region to complement the analysis presented here in the direction of understanding the dynamical properties responsible for the exacerbating dry conditions in the region.

Acknowledgments The authors thank D. Faranda, T. Grafke, F. Ragone, J. Wouters for many exchanges on extreme events, L. Recchia for her comments on a preliminary version of the manuscript, and two anonymous reviewers for constructive criticism. VL acknowledges the support by the Horizon 2020 project TiPES (grant no. 820970), by the Marie Curie ITN CriticalEarth (grant no. 956170) and by the EPSRC project EP/T018178/1. GM and JR acknowledge the European Research Council (ERC) under the European Union's Horizon 2020 research and innovation programme (project CENÆ: compound Climate Extremes in North America and Europe: from dynamics to predictability, grant no. 948309). VMG acknowledges the support of the Air, Water and Landscape Science Programme at the Department of Earth Sciences of Uppsala University.

-
- * Corresponding author. Email: v.lucarini@reading.ac.uk
- [1] A. AghaKouchak, L. Cheng, O. Mazdoyasani, and A. Farahmand. Global warming and changes in risk of concurrent climate extremes: Insights from the 2014 california drought. *Geophysical Research Letters*, 41(24):8847–8852, 2014.
 - [2] S. Bartusek, K. Kornhuber, and M. Ting. 2021 north american heatwave amplified by climate change-driven nonlinear interactions. *Nature Climate Change*, 12(12):1143–1150, 2022.
 - [3] R. Benzi, P. Malguzzi, A. Speranza, and A. Sutera. The statistical properties of general atmospheric circulation: Observational evidence and a minimal theory of bimodality. *Quarterly Journal of the Royal Meteorological Society*, 112(473):661–674, 1986.
 - [4] L. Bock, A. Lauer, M. Schlund, M. Barreiro, N. Belouin, C. Jones, G. A. Meehl, V. Predoi, M. J. Roberts, and V. Eyring. Quantifying progress across different cmip phases with the esmvaltool. *Journal of Geophysical Research: Atmospheres*, 125(21):e2019JD032321, 2020. e2019JD032321 2019JD032321.
 - [5] P. W. Chan, J. L. Catto, and M. Collins. Heatwave-blocking relation change likely dominates over decrease in blocking frequency under global warming. *npj Climate and Atmospheric Science*, 5(1):68, 2022.
 - [6] J. G. Charney and J. G. DeVore. Multiple flow equilibria in the atmosphere and blocking. *Journal of Atmospheric Sciences*, 36(7):1205 – 1216, 1979.
 - [7] J. G. Charney and D. M. Straus. Form-drag instability, multiple equilibria and propagating planetary waves in baroclinic, orographically forced, planetary wave systems. *Journal of Atmospheric Sciences*, 37(6):1157 – 1176, 1980.
 - [8] R. Chetrite and H. Touchette. Nonequilibrium markov processes conditioned on large deviations. *Annales Henri Poincaré*, 16(9):2005–2057, 2015.
 - [9] S. Coles. *An introduction to statistical modeling of extreme values*. Springer-Verlag, New York, 2001.
 - [10] G. Dematteis, T. Grafke, M. Onorato, and E. Vanden-Eijnden. Experimental evidence of hydrodynamic instantons: The universal route to rogue waves. *Phys. Rev. X*, 9:041057, Dec 2019.
 - [11] G. Dematteis, T. Grafke, and E. Vanden-Eijnden. Extreme event quantification in dynamical systems with random components. *SIAM/ASA Journal on Uncertainty Quantification*, 7(3):1029–1059, 2019.
 - [12] F. den Hollander. *Large Deviations*. American Mathematical Society, 2000.
 - [13] A. Di Luca, A. J. Pitman, and R. de Elía. Decomposing temperature extremes errors in cmip5 and cmip6 models. *Geophysical Research Letters*, 47(14):e2020GL088031, 2020. e2020GL088031 10.1029/2020GL088031.
 - [14] N. S. Diffenbaugh, D. L. Swain, and D. Touma. Anthropogenic warming has increased drought risk in california. *Proceedings of the National Academy of Sciences*, 112(13):3931–3936, 2015.
 - [15] R. Dole, M. Hoerling, J. Perlwitz, J. Eischeid, P. Pegion, T. Zhang, X.-W. Quan, T. Xu, and D. Murray. Was there a basis for anticipating the 2010 russian heat wave? *Geophysical Research Letters*, 38(6), 2011.
 - [16] D. R. Easterling, G. A. Meehl, C. Parmesan, S. A. Changnon, T. R. Karl, and L. O. Mearns. Climate extremes: Observations, modeling, and impacts. *Science*, 289(5487):2068–2074, 2000.
 - [17] V. Eyring, S. Bony, G. A. Meehl, C. A. Senior, B. Stevens, R. J. Stouffer, and K. E. Taylor. Overview of the Coupled Model Intercomparison Project Phase 6 (CMIP6) experimental design and organization. *Geoscientific Model Development*, 9:10539–10583, 2016.
 - [18] D. Faranda, V. Lucarini, P. Manneville, and J. Wouters. On using extreme values to detect global stability thresholds in multi-stable systems: The case of transitional plane couette flow. *Chaos, Solitons & Fractals*, 64:26–35, 2014.
 - [19] D. Faranda, G. Messori, A. Jézéquel, M. Vrac, and P. Yiou. Atmospheric circulation compounds anthropogenic warming and its impacts in Europe. preprint <https://hal.archives-ouvertes.fr/hal-0345653>, Nov 2021.
 - [20] D. Faranda, G. Messori, and P. Yiou. Dynamical proxies of north atlantic predictability and extremes. *Scientific Reports*, 7(1):41278, 2017.
 - [21] C. L. E. Franzke, A. Ciullo, E. A. Gilmore, D. M. Matias, N. Nagabhatla, A. Orlov, S. K. Paterson, J. Scheffran, and J. Sillmann. Perspectives on tipping points in integrated models of the natural and human earth system: cascading effects and telecoupling. *Environmental Research Letters*, 17(1):015004, jan 2022.
 - [22] V. M. Gálfi, T. Bódai, and V. Lucarini. Convergence of extreme value statistics in a two-layer quasi-geostrophic atmospheric model. *Complexity*, 2017:5340858, 2017.
 - [23] V. M. Galfi and V. Lucarini. Fingerprinting heatwaves and cold spells and assessing their response to climate change using large deviation theory. *Phys. Rev. Lett.*, 127:058701, Jul 2021.
 - [24] V. M. Gálfi, V. Lucarini, F. Ragone, and J. Wouters. Applications of large deviation theory in geophysical fluid dynamics and climate science. *La Rivista del Nuovo Cimento*, 44(6):291–363, 2021.
 - [25] C. Gessner, E. M. Fischer, U. Beyerle, and R. Knutti. Very rare heat extremes: Quantifying and understanding using ensemble reinitialization. *Journal of Climate*, 34(16):6619 – 6634, 2021.
 - [26] M. Ghil and V. Lucarini. The physics of climate variability and climate change. *Rev. Mod. Phys.*, 92:035002, Jul 2020.
 - [27] M. Ghil and A. W. Robertson. “waves” vs. “particles” in the atmosphere’s phase space: A pathway to long-range forecasting? *Proceedings of the National Academy of Sciences*, 99(suppl 1):2493–2500, 2002.
 - [28] A. Hannart, J. Pearl, F. E. L. Otto, P. Naveau, and M. Ghil. Causal counterfactual theory for the attribution of weather and climate-related events. *Bulletin of the American Meteorological Society*, 97(1):99 – 110, 2016.
 - [29] H. Hersbach, B. Bell, P. Berrisford, S. Hirahara, A. Horányi, J. Muñoz Sabater, J. Nicolas, C. Peubey, R. Radu, D. Schepers, A. Simmons, C. Soci, S. Abdalla, X. Abellan, G. Balsamo, P. Bechtold, G. Biavati, J. Bidlot, M. Bonavita, G. De Chiara, P. Dahlgren, D. Dee, M. Diamantakis, R. Dragani, J. Flemming, R. Forbes, M. Fuentes, A. Geer, L. Haimberger, S. Healy, R. J. Hogan, E. Hólm, M. Janisková, S. Keeley, P. Laloyaux, P. Lopez, C. Lupu, G. Radnoti, P. de Rosnay, I. Rozum, F. Vamborg, S. Villaume, and J.-N. Thépaut. The era5 global reanalysis. *Quarterly Journal of the Royal*

- Meteorological Society, 146(730):1999–2049, 2020.
- [30] A. L. Hirsch, N. N. Ridder, S. E. Perkins-Kirkpatrick, and A. Ukkola. Cmp6 multimodel evaluation of present-day heatwave attributes. *Geophysical Research Letters*, 48(22):e2021GL095161, 2021. e2021GL095161 2021GL095161.
- [31] A. Hochman, P. Alpert, T. Harpaz, H. Saaroni, and G. Messori. A new dynamical systems perspective on atmospheric predictability: Eastern mediterranean weather regimes as a case study. *Science Advances*, 5(6):eaau0936, 2019.
- [32] IPCC. *Managing the Risks of Extreme Events and Disasters to Advance Climate Change Adaptation*. Cambridge University Presse, 2012. [Field, C.B., V. Barros, T.F. Stocker, D. Qin, D.J. Dokken, K.L. Ebi, M.D. Mastrandrea, K.J. Mach, G.-K. Plattner, S.K. Allen, M. Tignor, and P.M. Midgley (eds.)]. A Special Report of Working Groups I and II of the Intergovernmental Panel on Climate Change.
- [33] B. Jiménez-Esteve and D. I. Domeisen. The role of atmospheric dynamics and large-scale topography in driving heatwaves. *Quarterly Journal of the Royal Meteorological Society*, 148(746):2344–2367, 2022.
- [34] B. Jiménez-Esteve, K. Kornhuber, and D. I. V. Domeisen. Heat extremes driven by amplification of phase-locked circumglobal waves forced by topography in an idealized atmospheric model. *Geophysical Research Letters*, 49(21):e2021GL096337, 2022. e2021GL096337 2021GL096337.
- [35] C. Koppe, R. Sari Kovats, B. Menne, G. Jendritzky, W. H. O. R. O. for Europe, L. S. of Hygiene, T. Medicine, E. European Commission. Energy, S. Development, and D. Wetterdienst. Heat-waves : risks and responses / by christina koppe ... [et al.], 2004.
- [36] K. Kornhuber, D. Coumou, E. Vogel, C. Lesk, J. F. Donges, J. Lehmann, and R. M. Horton. Amplified rossby waves enhance risk of concurrent heatwaves in major breadbasket regions. *Nature Climate Change*, 10(1):48–53, 2020.
- [37] W. K. M. Lau and K.-M. Kim. The 2010 Pakistan Flood and Russian Heat Wave: Teleconnection of Hydrometeorological Extremes. *Journal of Hydrometeorology*, 13(1):392–403, 02 2012.
- [38] R. Libonati, J. L. Geirinhas, P. S. Silva, A. Russo, J. A. Rodrigues, L. B. C. Belém, J. Nogueira, F. O. Roque, C. C. DaCamara, A. M. B. Nunes, J. A. Marengo, and R. M. Trigo. Assessing the role of compound drought and heatwave events on unprecedented 2020 wildfires in the pantanal. *Environmental Research Letters*, 17(1):015005, jan 2022.
- [39] H. Lin, R. Mo, and F. Vitart. The 2021 western north american heatwave and its subseasonal predictions. *Geophysical Research Letters*, 49, 03 2022.
- [40] E. N. Lorenz. Atmospheric predictability as revealed by naturally occurring analogues. *Journal of Atmospheric Sciences*, 26(4):636 – 646, 1969.
- [41] V. Lucarini, D. Faranda, A. de Freitas, J. de Freitas, M. Holland, T. Kuna, M. Nicol, M. Todd, and S. Vautenti. *Extremes and Recurrence in Dynamical Systems*. Pure and Applied Mathematics: A Wiley Series of Texts, Monographs and Tracts. Wiley, Hoboken, 2016.
- [42] V. Lucarini, V. M. Galfi, G. Messori, and J. Riboldi. Supplementary Material for "Typicality of the 2021 Western North America Summer Heatwave" by V. Lucarini, V. M. Galfi, G. Messori, and J. Riboldi. 12 2022.
- [43] V. Lucarini and A. Gritsun. A new mathematical framework for atmospheric blocking events. *Climate Dynamics*, 54(1):575–598, 2020.
- [44] P. Malguzzi, A. Speranza, A. Sutera, and R. Caballero. Nonlinear amplification of stationary rossby waves near resonance. part ii. *Journal of the Atmospheric Sciences*, 54(20):2441 – 2451, 1997.
- [45] M. E. Mann and P. H. Gleick. Climate change and california drought in the 21st century. *Proceedings of the National Academy of Sciences*, 112(13):3858–3859, 2015.
- [46] MATLAB. *Version R2020a*. The MathWorks Inc., Natick, Massachusetts, 2020.
- [47] M. Matsueda and T. Palmer. Estimates of flow-dependent predictability of wintertime euroatlantic weather regimes in medium-range forecasts. *Quarterly Journal of the Royal Meteorological Society*, 144(713):1012–1027, 2018.
- [48] T. Mauritsen, J. Bader, T. Becker, J. Behrens, M. Bittnner, R. Brokopf, V. Brovkin, M. Claussen, T. Crueger, M. Esch, I. Fast, S. Fiedler, D. Fläschner, V. Gayler, M. Giorgetta, D. S. Goll, H. Haak, S. Hagemann, C. Hedemann, C. Hohenegger, T. Ilyina, T. Jahns, D. Jimenez-de-la Cuesta, J. Jungclaus, T. Kleinen, S. Kloster, D. Kracher, S. Kinne, D. Kleberg, G. Lasslop, L. Kornblueh, J. Marotzke, D. Matei, K. Meraner, U. Mikolajewicz, K. Modali, B. Möbis, W. A. Müller, J. E. M. S. Nabel, C. C. W. Nam, D. Notz, S.-S. Nyawira, H. Paulsen, K. Peters, R. Pincus, H. Pohlmann, J. Pongratz, M. Popp, T. J. Raddatz, S. Rast, R. Redler, C. H. Reick, T. Rohrschneider, V. Schemann, H. Schmidt, R. Schnur, U. Schulzweida, K. D. Six, L. Stein, I. Stemmler, B. Stevens, J.-S. von Storch, F. Tian, A. Voigt, P. Vrese, K.-H. Wieners, S. Wilkenskjaeld, A. Winkler, and E. Roeckner. Developments in the mpi-m earth system model version 1.2 (mpi-esm1.2) and its response to increasing co2. *Journal of Advances in Modeling Earth Systems*, 11(4):998–1038, 2019.
- [49] G. J. McLachlan and D. Peel. *Finite mixture models*. Wiley, New York, 2000.
- [50] D. G. Miralles, A. J. Teuling, C. C. van Heerwaarden, and J. Vilà-Guerau de Arellano. Mega-heatwave temperatures due to combined soil desiccation and atmospheric heat accumulation. *Nature Geoscience*, 7(5):345–349, 2014.
- [51] S. L. Mullen. The impact of orography on blocking frequency in a general circulation model. *Journal of Climate*, 2(12):1554 – 1560, 1989.
- [52] V. Narinesingh, J. F. Booth, S. K. Clark, and Y. Ming. Atmospheric blocking in an aquaplanet and the impact of orography. *Weather and Climate Dynamics*, 1(2):293–311, 2020.
- [53] M. Osman, B. F. Zaitchik, and N. S. Winstead. Cascading drought-heat dynamics during the 2021 southwest united states heatwave. *Geophysical Research Letters*, 49(12):e2022GL099265, 2022. e2022GL099265 2022GL099265.
- [54] J. L. Pelly and B. J. Hoskins. A new perspective on blocking. *Journal of the Atmospheric Sciences*, 60(5):743 – 755, 2003.
- [55] S. Y. Philip, S. F. Kew, G. J. van Oldenborgh, F. S. Anslow, S. I. Seneviratne, R. Vautard, D. Coumou, K. L. Ebi, J. Arrighi, R. Singh, M. van Aalst, C. Pereira Marghidan, M. Wehner, W. Yang, S. Li,

- D. L. Schumacher, M. Hauser, R. Bonnet, L. N. Luu, F. Lehner, N. Gillett, J. S. Tradosky, G. A. Vecchi, C. Rodell, R. B. Stull, R. Howard, and F. E. L. Otto. Rapid attribution analysis of the extraordinary heat wave on the pacific coast of the us and canada in june 2021. *Earth System Dynamics*, 13(4):1689–1713, 2022.
- [56] M. Poumadère, C. Mays, S. Le Mer, and R. Blong. The 2003 heat wave in france: Dangerous climate change here and now. *Risk Analysis*, 25(6):1483–1494, 2005.
- [57] F. Ragone and F. Bouchet. Rare event algorithm study of extreme warm summers and heatwaves over europe. *Geophysical Research Letters*, 48(12):e2020GL091197, 2021. e2020GL091197 2020GL091197.
- [58] F. Ragone, J. Wouters, and F. Bouchet. Computation of extreme heat waves in climate models using a large deviation algorithm. *Proceedings of the National Academy of Sciences*, 2017.
- [59] P. M. Ruti, V. Lucarini, A. Dell’Aquila, S. Calmanti, and A. Speranza. Does the subtropical jet catalyze the midlatitude atmospheric regimes? *Geophysical Research Letters*, 33(6), 2006.
- [60] S. Schubert and V. Lucarini. Dynamical analysis of blocking events: spatial and temporal fluctuations of covariant lyapunov vectors. *Quarterly Journal of the Royal Meteorological Society*, 142(698):2143–2158, 2016.
- [61] D. L. Schumacher, J. Keune, C. C. van Heerwaarden, J. Vilà-Guerau de Arellano, A. J. Teuling, and D. G. Miralles. Amplification of mega-heatwaves through heat torrents fuelled by upwind drought. *Nature Geoscience*, 12(9):712–717, 2019.
- [62] R. Seager, M. Hoerling, S. Schubert, H. Wang, B. Lyon, A. Kumar, J. Nakamura, and N. Henderson. Causes of the 2011-14 california drought. *Journal of Climate*, 28(18):6997 – 7024, 2015.
- [63] S. J. Sutanto, C. Vitolo, C. Di Napoli, M. D’Andrea, and H. A. Van Lanen. Heatwaves, droughts, and fires: Exploring compound and cascading dry hazards at the pan-european scale. *Environment International*, 134:105276, 2020.
- [64] D. L. Swain. A tale of two california droughts: Lessons amidst record warmth and dryness in a region of complex physical and human geography. *Geophysical Research Letters*, 42(22):9999–10,003, 2015.
- [65] K. E. Taylor. Summarizing multiple aspects of model performance in a single diagram. *Journal of Geophysical Research: Atmospheres*, 106(D7):7183–7192, 2001.
- [66] H. Teng and G. Branstator. Causes of extreme ridges that induce california droughts. *Journal of Climate*, 30(4):1477 – 1492, 2017.
- [67] V. Thompson, A. T. Kennedy-Asser, E. Vosper, Y. T. E. Lo, C. Huntingford, O. Andrews, M. Collins, G. C. Hegerl, and D. Mitchell. The 2021 western north america heat wave among the most extreme events ever recorded globally. *Science Advances*, 8(18):eabm6860, 2022.
- [68] R. Tibshirani, G. Walther, and T. Hastie. Estimating the number of clusters in a data set via the gap statistic. *Journal of the Royal Statistical Society: Series B (Statistical Methodology)*, 63(2):411–423, 2001.
- [69] H. Touchette. The large deviation approach to statistical mechanics. *Physics Reports*, 478:1–69, 2009.
- [70] S. Varadhan. *Large Deviations and Applications*. SIAM, Philadelphia, 1984.
- [71] R. Vautard and P. Yiou. Control of recent european surface climate change by atmospheric flow. *Geophysical Research Letters*, 36(22), 2009.
- [72] S. S. Wang, L. Zhao, J.-H. Yoon, P. Klotzbach, and R. R. Gillies. Quantitative attribution of climate effects on hurricane harvey’s extreme rainfall in texas. *Environmental Research Letters*, 13(5):054014, 2018.
- [73] T. Woollings, D. Barriopedro, J. Methven, S.-W. Son, O. Martius, B. Harvey, J. Sillmann, A. R. Lupo, and S. Seneviratne. Blocking and its response to climate change. *Current Climate Change Reports*, 4(3):287–300, 2018.
- [74] M. Zampieri, F. D’Andrea, R. Vautard, P. Ciais, N. de Noblet-Ducoudre, and P. Yiou. Hot european summers and the role of soil moisture in the propagation of mediterranean drought. *Journal of Climate*, 22(18):4747 – 4758, 2009.
- [75] F. Zhang, J. A. Biederman, M. P. Dannenberg, D. Yan, S. C. Reed, and W. K. Smith. Five decades of observed daily precipitation reveal longer and more variable drought events across much of the western united states. *Geophysical Research Letters*, 48(7):e2020GL092293, 2021. e2020GL092293 2020GL092293.
- [76] W. Zhang, V. Hari, S. S-Y Wang, M. D. LaPlante, G. Garfin, G. Affram, and R. Kumar. Fewer troughs, not more ridges, have led to a drying trend in the western united states. *Geophysical Research Letters*, 49(1):e2021GL097089, 2022. e2021GL097089 2021GL097089.
- [77] E. Zorita and H. von Storch. The analog method as a simple statistical downscaling technique: Comparison with more complicated methods. *Journal of Climate*, 12(8):2474 – 2489, 1999.